Rare Metal Materials and Engineering
Volume 53, Issue 4, April 2024
Available online at www.rmme.ac.cn

Science Press

Cite this article as: Li Junwei, Jia Weimin, Liu Chong, et al. First-Principles and *ab*-initio Molecular Dynamics Simulation Research on Adsorption and Dissociation of CO and CO_2 Molecules on UO_2 (111) Slab[J]. Rare Metal Materials and Engineering, 2024, 53(04): 933-946. DOI: 10.12442/j.issn.1002-185X.20230402.

ARTICLE

First-Principles and *ab*-initio Molecular Dynamics Simulation Research on Adsorption and Dissociation of CO and CO_2 Molecules on UO_2 (111) Slab

Li Junwei[1,2], Jia Weimin[2], Liu Chong[1], Li Peiyao[1], Li Zhengcao[1]

[1] School of Materials Science and Engineering, Tsinghua University, Beijing 100084, China; [2] Xi'an Research Institute of High-Technology, Xi'an 710025, China

Abstract: The adsorption and dissociation of CO and CO_2 molecules on UO_2 (111) slab were investigated by the first-principles calculations based on density functional theory with the addition of Hubbard term for calculation correction. Different static and dynamic adsorption mechanisms under different configurations were analyzed, and the adsorption sites included top, hollow, and bridge sites. In the static calculations, the variation of adsorption parameters, such as adsorption configuration, adsorption energy, and charge transfer, during adsorption process was investigated. *ab*-initio molecular dynamics (AIMD) was employed to study the dissociation process of CO_2 molecules and the changes in charge density difference. Results show that the adsorption of CO molecules can be categorized into two types: (1) stable adsorption, including chemical and physical adsorptions; (2) unstable adsorption. The adsorption types of CO_2 on UO_2 (111) slab only include the chemical adsorption of stable adsorption and unstable adsorption. No physical adsorption exists. The optimal configuration for the adsorption of both CO and CO_2 molecules is short-bridge vertical (B-short-Ver) adsorption. Additionally, at 0 K, the CO_2 molecules at the configurations related to B-short-Ver adsorption and long-bridge vertical adsorption on UO_2 (111) slab spontaneously dissociate after adsorption. AIMD simulation results show that both configurations dissociate at 300 K.

Key words: uranium dioxide; chemical adsorption; DFT+U; bridge vertical

Uranium dioxide (UO_2) is a widely used nuclear fuel in the nuclear reactors due to its high energy generation through fission reactions. Thus, the physical, chemical, optical, and thermodynamic properties of UO_2 have been extensively studied by experiments and theoretical techniques[1–4]. The performance of UO_2 has been investigated under harsh environment conditions, including high temperature, high pressure, and large radiation dose[5–9]. Noble gas impurities and various defects exist in UO_2, such as He[10], Ne[11], Ar[12], Kr[13], and Xe[14]. For example, He is a noble gas produced by the fission reaction of uranium, which tends to accumulate in the bubbles, causing fuel swelling, surface bulging, and high-temperature embrittlement. UO_2 thin films can be used in space exploration, such as space telescopes and multilayer mirrors[15]. Their optical properties, such as reflectivity, refractive index, and energy-loss spectrum, have also been widely investigated[16].

Surface corrosion is a fundamental problem in the application of UO_2 due to its unique electronic structure and strong correlation of 5f electrons of uranium[17]. Weck et al[18] conducted the corrosion investigation on UO_2 fuel and revealed the oxidation from U^{4+} into U^{6+} in water environment or with other oxidization agents. Uranium-based alloys are also prone to surface corrosion, including hydrogen corrosion and oxidation[19–20]. For instance, rapid oxidation occurs on the uranium surface during the short transfer from vacuum environment, resulting in the formation of uranium oxide on the surface of depleted uranium and its alloys. The thickness of the uranium oxide layer is increased with prolonging the oxidation time, leading to severe inward corrosion and even

Received date: June 26, 2023
Foundation item: National Natural Science Foundation of China (11975135, 12005017); National Basic Research Program of China (2020YFB1901800)
Corresponding author: Li Zhengcao, Ph. D., Professor, School of Materials Science and Engineering, Tsinghua University, Beijing 100084, P. R. China, Tel: 0086-10-62772233, E-mail: zcli@tsinghua.edu.cn

material failure. The investigation of surface corrosion mechanism is crucial to improve the corrosion resistance of UO_2 and uranium-based alloys. Oxidation rate and oxidation products of UO_2 under different reaction conditions (temperature and duration) have been widely researched[21–22]. However, the evolution behavior of each reaction process can hardly be captured in experiments, not to mention the microstructure changes at different stages.

Atomic-scale mechanism is essential for the integrated mechanism of UO_2 surface corrosion. Theoretical calculations, particularly density functional theory (DFT), have been proven to be effective tools to investigate the atomic-scale mechanisms. The electronic structure of UO_2 has been extensively studied by DFT calculations[23–24]. DFT calculation results indicate that UO_2 is a Mott-Hubbard insulator. However, the early DFT calculations cannot capture the Mott-Hubbard insulator state due to inadequate descriptions of Coulomb and exchange interactions[25]. Subsequent calculations incorporate the Hubbard U (DFT+U) correction term to accurately describe UO_2 as an insulator. The appropriate Hubbard U value has been discussed to ensure that the ground state parameters, such as band gap and density of states (DOS), can closely align with the experiment results[16,26]. Chen et al[16] compiled the band gap values of UO_2 from various calculation results and depicted the band gap as a function of Hubbard value in DFT calculation.

Most researches about the UO_2 surface properties focus on the low-index crystal surfaces, such as (111), (110), and (100) slabs, which use quantum-mechanical surface energy calculations to determine their relative stabilities[27]. Among the low-index crystal surfaces, (111) slab is the most stable one according to DFT calculations and it serves as the primary surface for the study in adsorption, dissociation, and initial stage surface corrosion[28]. Extensive investigations have been conducted on the oxidation, adsorption, dissociation, and diffusion of O_2 and H_2O molecules on UO_2 (111) slab[29–30]. However, the theoretical research on the adsorption of CO and CO_2 molecules on UO_2 (111) slab is rarely reported, which is also relevant to UO_2 oxidation.

In this research, the static and dynamic behavior was investigated based on the adsorption and dissociation of CO and CO_2 molecules on UO_2 (111) slab. The UO_2 unit cell was used to construct the UO_2 (111) slab. Static calculations were then performed to analyze the adsorption configurations, adsorption energies, bonding types, and charge transfer at five highly symmetrical adsorption sites. Additionally, crystal orbital Hamiltonian population (COHP), total density of states (TDOS), and partial density of states (PDOS) were analyzed in the optimized adsorption configurations to elucidate the oxidation mechanism on UO_2 surface. This research also investigated the structure evolution and charge density differences in the specific configurations related to the CO and CO_2 adsorption on UO_2 (111) slab at 300 K using *ab*-initio molecular dynamics (AIMD).

1 Methods

Electronic structure calculations were performed by DFT calculations implemented in the Vienna *ab*-initio simulation package (VASP 5.4.4) [31–32]. The exchange and correlation energies of electrons are treated by generalized gradient approximation (GGA) based on the Perdew-Burke-Ernzerhof (PBE) exchange-correlation potential[33–34]. The valence electron configurations for the U, O, and C atoms are $6s^26p^67s^25f^36d^1$, $2s^22p^4$, and $2s^22p^2$, respectively. To calculate the electron-electron correlation of UO_2, the DFT+U method was employed. The correlation (U) and exchange (J) parameters were set independently, and only the difference (U_{eff}) between U and J was required in VASP software. The value of U_{eff} ranged from 3.3 eV to 4.1 eV[16,35], leading to the good consistence between the experiment observations and the *ab*-initio simulation results. In this research, U_{eff} was set as 3.5 eV, and the spin polarization was also considered in the calculation.

The unit cell of UO_2 containing 12 atoms was optimized by a 11×11×11 Monkhorst-Pack k-point mesh[36] for Brillouin zone integration. Specifically, the unit cell represented a collinear antiferromagnetic (AFM) structure with the initial magnitude of uranium atom as 2 μB in UO_2. The plane wave cutoff was set as 500 eV. The calculated lattice parameter was 0.5559 nm, which was in good agreement with the experiment value of 0.5468 nm[37]. Additionally, the calculation results aligned well with the results in Ref.[10,38–39]. Fig.1 shows the optimized unit cell structure of UO_2, which exhibits the fluorite (CaF_2) structure. TDOS and PDOS are shown in Fig.2, as well as the Fermi level energy E_F. It is reported that UO_2 is a non-metal material. The calculated band gap of 1.84 eV closely corresponds to the findings in Ref.[16,38,40], although it is slightly lower than the experiment result of 2.1 eV[41].

The valence band consists of U 6p, U 6d, U 5f, and O 2p orbitals, whereas the conduction band is formed by U 6d and U 5f orbitals, as shown in Fig. 2b. The optimized lattice parameter of the UO_2 unit cell was used to construct the UO_2 (111) slab. In this calculation, the bottom three layers were fixed to simulate the substrate atoms of UO_2 (111) slab, whereas the top two layers were relaxed to simulate the surface atoms.

Fig. 3 shows side and top views of UO_2 (111) slab after

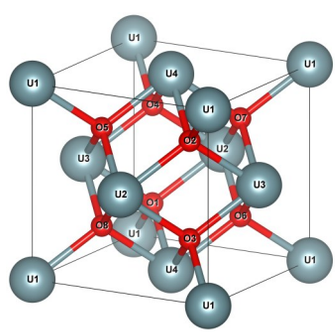

Fig.1 Optimized unit cell structure of UO_2

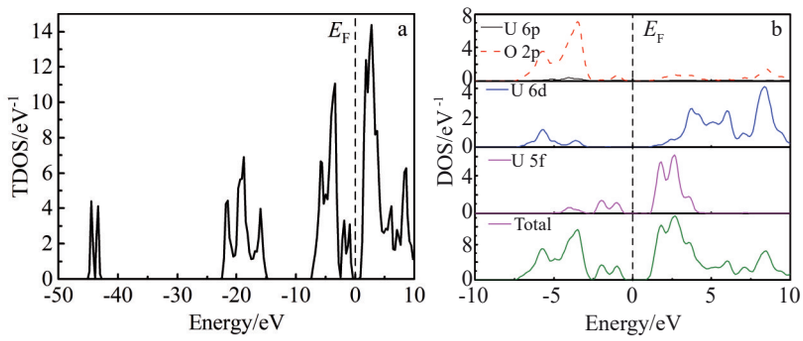

Fig.2 TDOS (a) and DOS (b) of UO_2 unit cell

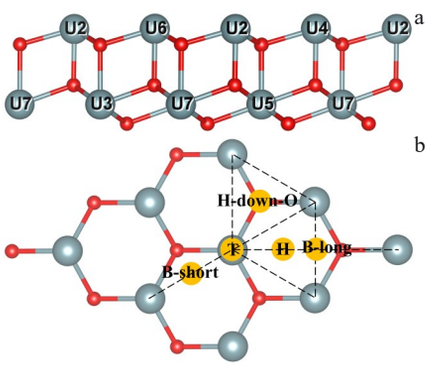

Fig.3 Side (a) and top (b) views of UO_2 (111) slab with five highly symmetrical adsorption sites after structure optimization

structure optimization with five highly symmetrical adsorption sites (top, hollow, and bridge sites). In the following discussion and schematic diagrams in this research, blue-gray, brown, and red balls represent the uranium, carbon, and oxygen atoms, respectively. T represents the top site for the surface U atom; H represents the center site of a triangle enclosed by three adjacent surface U atoms; H-down-O represents the center site of a triangle enclosed by three adjacent surface U atoms with an oxygen atom at the subsurface site; B-short represents the bridge site of U atoms on the adjacent surface; B-long represents the bridge site of U atoms on the sub-adjacent surface. Additionally, the dipole correction was applied to eliminate the effect of dipole moment[42]. A vacuum region with 1.5 nm in length along the *z*-axis was included to separate the periodic images in this calculation.

2 Results and Discussion

2.1 Adsorption energy and configuration

Fig. 4 illustrates top and side views of CO molecules with different adsorption configurations on UO_2 (111) slab before structure relaxation. There are five highly symmetrical adsorption sites, and each site involves three situations: (1) CO molecule positioned horizontally to the UO_2 (111) slab (Hor); (2) CO molecule positioned vertically to the UO_2 (111) slab with C atom closer to the surface (Ver); (3) CO molecule positioned vertically to the UO_2 (111) slab with O atom closer to the surface (Ver-O). Therefore, fifteen configurations of CO adsorption are presented in Fig. 4. The abbreviations for different adsorption configurations are as follows: T-Ver-O represents the top vertical site with the O atom closer to the surface; H-Hor represents the hollow horizontal site; B-short-Ver represents the short bridge vertical site. CO molecule is optimized in a box with dimension of 1 nm×1 nm×1 nm. The calculated bond length of 0.1144 nm aligns well with the experiment value of 0.1129 nm. Fig. 5 displays the top and side views of CO molecules with different adsorption configurations on UO_2 (111) slab after structure relaxation. It can be observed that apart from the T-Ver, T-Ver-O, H-down-O-Ver, and H-down-O-Ver-O configurations, the C and O atoms of CO molecule with other configurations can bond to the surface U atoms. There is no evidence of CO molecule dissociation after structure optimization in all adsorption configurations. The bonding adsorption of CO molecule can only be observed along the horizontal direction in the initial top and H-down-O configurations. No bonding adsorption can be observed along the vertical direction, suggesting that CO adsorption on the surface along vertical direction is difficult.

Table 1 presents the adsorption energy and geometrical parameters of CO molecule adsorption on the UO_2 (111) slab for all configurations. E_{ads} represents the adsorption energy; $d_{C\text{-}O}$ represents the distance between C and O atoms of CO molecule; Bond C represents the C atom bonding with the slab surface atom; Bond O represents the O atom of CO molecule bonding with the slab surface atom; $d_{Bond\ C}$ represents the bond length between slab surface atom and C atom; $d_{Bond\ O}$ represents the bond length between slab surface atom and O atom. The adsorption energy E_{ads} can be obtained by Eq.(1), as follows:

$$E_{ads} = E_{slab+mol} - E_{slab} - E_{mol} \quad (1)$$

where $E_{slab+mol}$ represents the total energy for adsorption system after CO adsorption, E_{slab} represents the total energy of UO_2 (111) slab, and E_{mol} represents the CO molecule energy. The negative adsorption energy indicates the stable adsorption system. The larger the absolute value of adsorption energy, the more stable the adsorption system. Conversely, positive adsorption energy suggests that the adsorption system becomes unstable.

It is observed that the distance between the C and O atoms of the CO molecule ($d_{C\text{-}O}$) increases compared with the bond

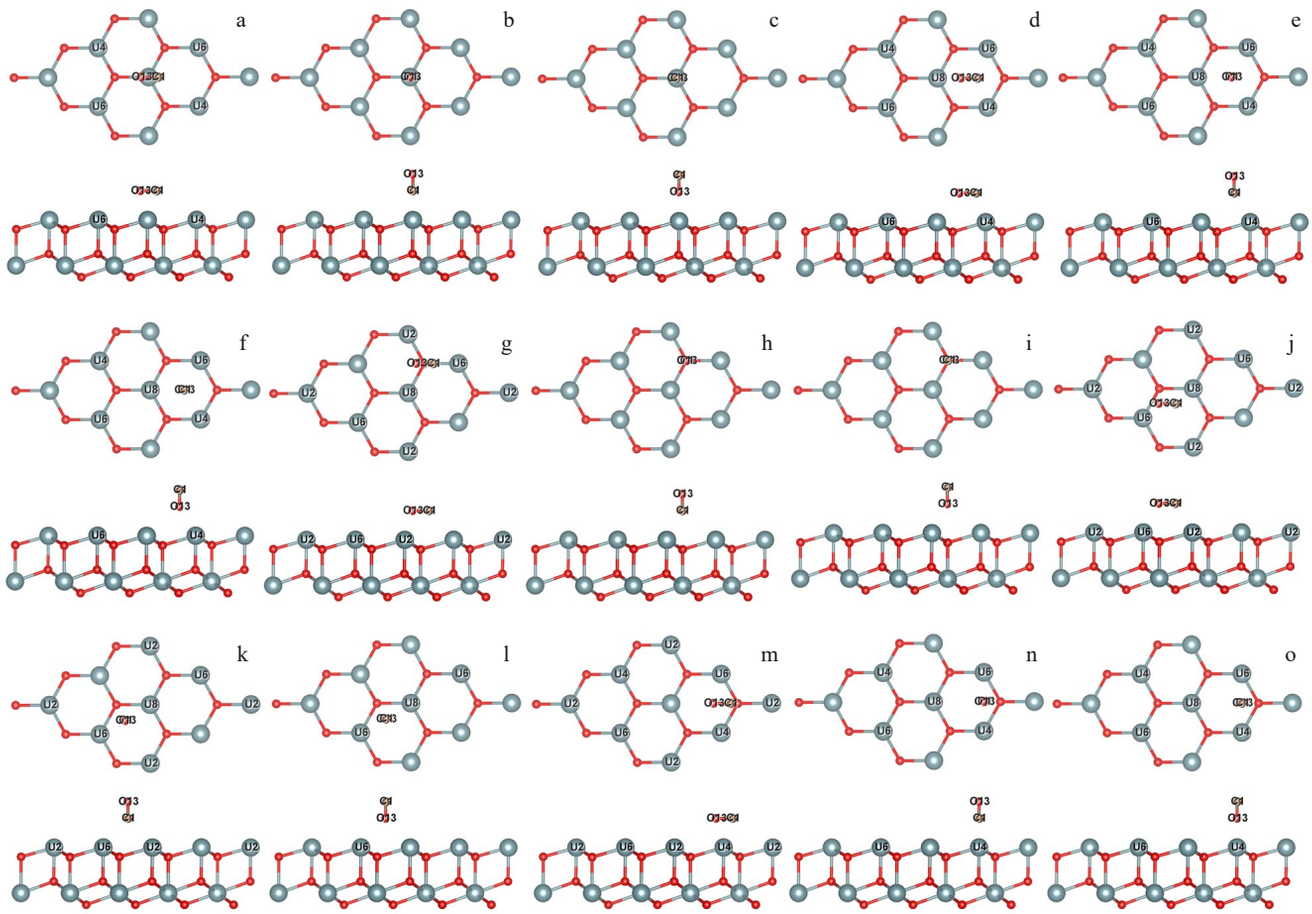

Fig.4 Top and side views of CO molecules with different adsorption configurations on UO_2 (111) slab before structure relaxation: (a) T-Hor; (b) T-Ver; (c) T-Ver-O; (d) H-Hor; (e) H-Ver; (f) H-Ver-O; (g) H-down-O-Hor; (h) H-down-O-Ver; (i) H-down-O-Ver-O; (j) B-short-Hor; (k) B-short-Ver; (l) B-short-Ver-O; (m) B-long-Hor; (n) B-long-Ver; (o) B-long-Ver-O

length of the free CO molecule after adsorption. This phenomenon results in the decrease in the strength of C-O bonding. Except that of the T-Ver-O and H-down-O-Ver-O configurations, the adsorption energy of all configurations is negative, indicating the stable adsorption of the CO molecule on the UO_2 (111) slab. Specifically, the T-Ver and H-down-O-Ver configurations demonstrate the physical adsorption without bonding to the slab atoms.

Fig.6 and Fig.7 show the configurations of the top and side views of CO_2 molecule adsorption on the UO_2 (111) slab before and after structure relaxation, respectively. CO_2 molecule is optimized before structure optimization. The C=O bond length (0.1176 nm) agrees well with the experiment value (0.1162 nm)[43]. Except those in the T-Ver, H-Ver, and H-down-O-Ver configurations, the O atoms of CO_2 molecule bond to the surface U atoms in all other configurations. However, after structure optimization, the CO_2 molecule dissociates in the B-short-Ver and B-long-Ver configurations, and only C atoms bond to the surface U atoms in these two configurations. Table 2 presents the adsorption energy and geometric parameters of the CO_2 molecule adsorption on the UO_2 (111) slab. $d_{C\text{-}O1}/d_{C\text{-}O2}$ represents the distance between C atom and O1 atom/O2 atom of CO molecule; $\theta_{O\text{-}C\text{-}O}$ represents the bond angle with the CO_2 molecule between the C atom and O1 and O2 atoms. Similar to the CO molecule adsorption, the $d_{C\text{-}O1}$ and $d_{C\text{-}O2}$ values increase, compared with the bond length of C=O at free state after adsorption. The CO_2 molecule deviates from its linear structure, resulting in a weakened C=O bond interaction due to the CO_2 adsorption.

Similar results are observed for CO and CO_2 molecule adsorption on the UO_2 (111) slab. The adsorption stability of bridge sites, including the short and long bridge configurations, is better than that of other sites, indicating the chemical adsorption of CO and CO_2 molecules on the bridge sites of the UO_2 (111) slab. Thus, the initial B-short-Ver configuration is optimal for both CO and CO_2 molecule adsorption on the UO_2 (111) slab. In CO molecule adsorption, the system stability of Hor, Ver, and Ver-O configurations gradually decreases. In CO_2 molecule adsorption, the system stability of Hor and Ver configurations gradually decreases. The bond lengths between the C atoms and surface U atoms range from 0.2287 nm to 0.2501 nm in the CO adsorption and from 0.2282 nm to 0.2520 nm in CO_2 adsorption on the UO_2 (111) slab, as indicated in Table 1 and Table 2. These values

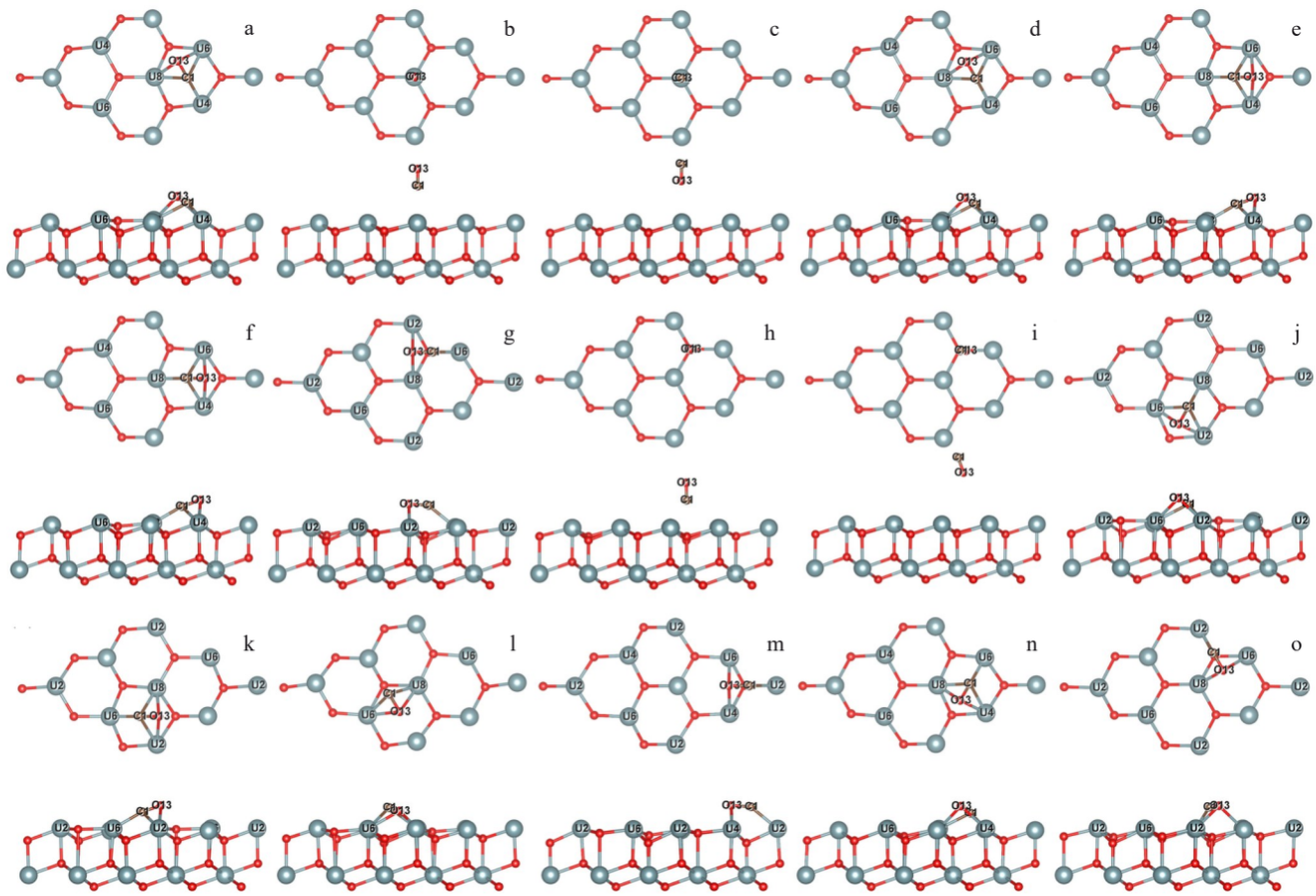

Fig.5 Top and side views of CO molecules with different adsorption configurations on UO_2 (111) slab after structure relaxation: (a) T-Hor; (b) T-Ver; (c) T-Ver-O; (d) H-Hor; (e) H-Ver; (f) H-Ver-O; (g) H-down-O-Hor; (h) H-down-O-Ver; (i) H-down-O-Ver-O; (j) B-short-Hor; (k) B-short-Ver; (l) B-short-Ver-O; (m) B-long-Hor; (n) B-long-Ver; (o) B-long-Ver-O

are close to the bond length of U-C in UC (0.2480 nm) [44]. Additionally, the bond lengths between the O atoms and surface U atoms range from 0.2402 nm to 0.2504 nm in CO adsorption and from 0.2258 nm to 0.2566 nm in CO_2 adsorption, which are closer to the bond length of U-O in UO_2 (0.2370 nm) [37]. These results demonstrate the formation of stable chemical bonds between the C or O atoms and the U atoms on the slab.

However, the adsorption types of CO and CO_2 molecule absorption on UO_2 (111) slab are different. CO adsorption includes stable adsorption (both chemical and physical adsorption) as well as unstable adsorption. CO_2 adsorption only consists of stable adsorption of chemical adsorption and unstable adsorption. Chemical adsorption leads to the bonding between the surface U atoms and the C or O atoms in the CO_2 molecule.

2.2 Charge distribution

Table 3 and Table 4 present the net charge distribution numbers for CO and CO_2 adsorption on the UO_2 (111) slab, respectively. q_C and q_O are net charge numbers of C and O atom, respectively; $q_{\text{total CO}}$ is the sum net charge number of C and O atoms of CO molecules; q_{1st}, q_{2nd}, q_{3rd}, q_{4th}, and q_{5th} are the total net charge numbers of the first, second, third, fourth, and fifth layers on slab, respectively; q_{O1} and q_{O2} are net charge numbers of O1 and O2 atoms, respectively; $q_{\text{total CO}_2}$ is the sum net charge number of O1, O2, and C atoms of CO_2 molecules. The UO_2 (111) slab transfers net charge to the CO and CO_2 molecules, and the surface layer is the primary supplier of electrons compared with other layers of the UO_2 (111) slab. This phenomenon can also be observed in the adsorption process of other small molecules[28]. Furthermore, the charge transfer is greater in the dissociated adsorption, compared with that of the associated adsorption. Notably, the B-short-Ver configuration exhibits the highest charge accumulation in the adsorption of both CO and CO_2 molecules. In the stable adsorption of CO and CO_2 molecules on the UO_2 (111) slab, the C atoms gain more charge than the O atoms do. This is because the energy level of the C atomic orbital is closer to that of the 2π* molecular orbital which is composed of the p atomic orbitals of the C and O atoms in the CO molecule. Consequently, the transferred electrons primarily concentrate on the C atoms during CO molecule adsorption. Since the highest occupied molecular orbital (HOMO) is related to the lone pair of electrons provided by O atoms, the presence of surrounding electrons weakens the electron adsorption ability of O atoms. Therefore, electrons

Table 1 Adsorption energy and geometrical parameters of CO molecule adsorption on UO_2 (111) slab

Configuration	E_{ads}/eV	d_{C-O}/nm	Bond C	$d_{Bond\ C}$/nm	Bond O	$d_{Bond\ O}$/nm
T-Hor	−2.038	0.1382	C-U_4	0.2294	O-U_6	0.2413
			C-U_6	0.2478	O-U_8	0.2467
			C-U_8	0.2496	-	-
T-Ver	−0.667	0.1171	-	-	-	-
T-Ver-O	0.489	0.1153	-	-	-	-
H-Hor	−2.333	0.1386	C-U_4	0.2292	O-U_6	0.2403
			C-U_6	0.2471	O-U_8	0.2466
			C-U_8	0.2493	-	-
H-Ver	−2.118	0.1369	C-U_4	0.2492	O-U_4	0.2454
			C-U_6	0.2497	O-U_6	0.2460
			C-U_8	0.2289	-	-
H-Ver-O	−1.976	0.1365	C-U_4	0.2500	O-U_4	0.2458
			C-U_6	0.2495	O-U_6	0.2455
			C-U_8	0.2287	-	-
H-down-O-Hor	−1.771	0.1348	C-U_6	0.2380	O-U_2	0.2481
			-	-	O-U_8	0.2482
H-down-O-Ver	−0.738	0.1196	-	-	-	-
H-down-O-Ver-O	0.458	0.1145	-	-	-	-
B-short-Hor	−2.437	0.1386	C-U_2	0.2469	O-U_2	0.2406
			C-U_6	0.2493	O-U_6	0.2466
			C-U_8	0.2290	-	-
B-short-Ver	−2.572	0.1369	C-U_2	0.2490	O-U_2	0.2456
			C-U_6	0.2291	O-U_8	0.2463
			C-U_8	0.2497	-	-
B-short-Ver-O	−1.067	0.1405	C-U_6	0.2501	O-U_6	0.2504
			C-U_8	0.2489	O-U_8	0.2466
B-long-Hor	−1.437	0.1352	C-U_2	0.2379	O-U_4	0.2478
			-	-	O-U_6	0.2483
B-long-Ver	−1.939	0.1379	C-U_4	0.2483	O-U_4	0.2478
			C-U_6	0.2298	O-U_8	0.2402
			C-U_8	0.2430	-	-
B-long-Ver-O	−0.989	0.1346	C-U_2	0.2380	O-U_6	0.2452
			-	-	O-U_8	0.2486

preferentially transfer through the C atoms of CO_2 molecules.

Fig. 8 illustrates the change in the absolute value of adsorption energy E_{ads} with the charge gain in the adsorption of CO and CO_2 molecules on the UO_2 (111) slab. The absolute value of E_{ads} is increased with increasing the charge gain for both CO and CO_2 molecules, indicating the positive correlation between adsorption stability and charge gain. Additionally, the absolute value of E_{ads} is larger for CO_2 adsorption, compared with that of CO adsorption at the same charge gain situation. This result suggests that CO adsorption exhibits better stability than CO_2 adsorption does at the same charge gain situation.

2.3 Distribution of Bader charge

COHP[45] was investigated in the optimized configurations of CO and CO_2 molecules, and the results are obtained by LOBSTER program[46–47], shown in Fig. 9. The positive and negative COHP values correspond to the bonding and antibonding interactions, respectively. According to Fig. 9, the −COHP values which are positive with corresponding energies below the Fermi level indicate the bonding interactions between the CO/CO_2 molecules and the UO_2 (111) slab. The integral result of COHP value below the Fermi level is denoted as ICOHP, which reflects the strength of corresponding atom interactions. Table 5 presents ICOHP values for the C and O atoms with the surface bonding atoms. ICOHP-C represents the ICOHP value for C atom with surface atom, and ICOHP-O represents the ICOHP value for O atom with surface atom. The total ICOHP value in the CO_2 adsorption with B-short-Ver configuration is larger than that in the CO adsorption with B-short-Ver configuration, suggesting

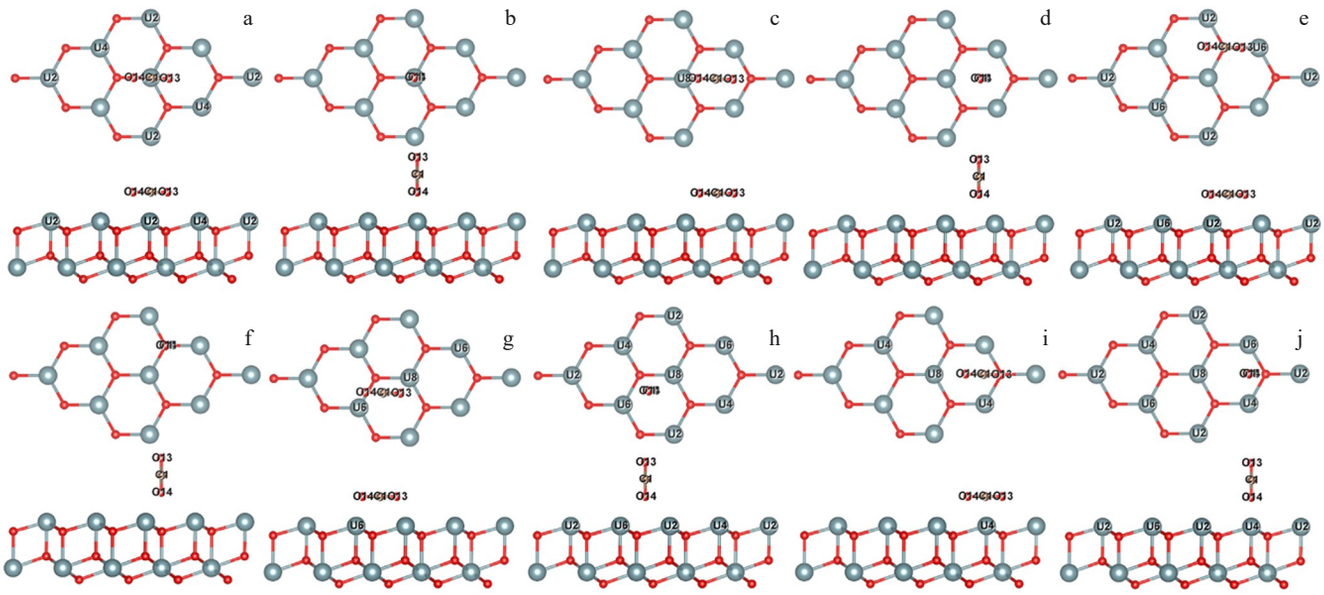

Fig.6 Top and side views of CO_2 molecules with different adsorption configurations on UO_2 (111) slab before structure relaxation: (a) T-Hor; (b) T-Ver; (c) H-Hor; (d) H-Ver; (e) H-down-O-Hor; (f) H-down-O-Ver; (g) B-short-Hor; (h) B-short-Ver; (i) B-long-Hor; (j) B-long-Ver

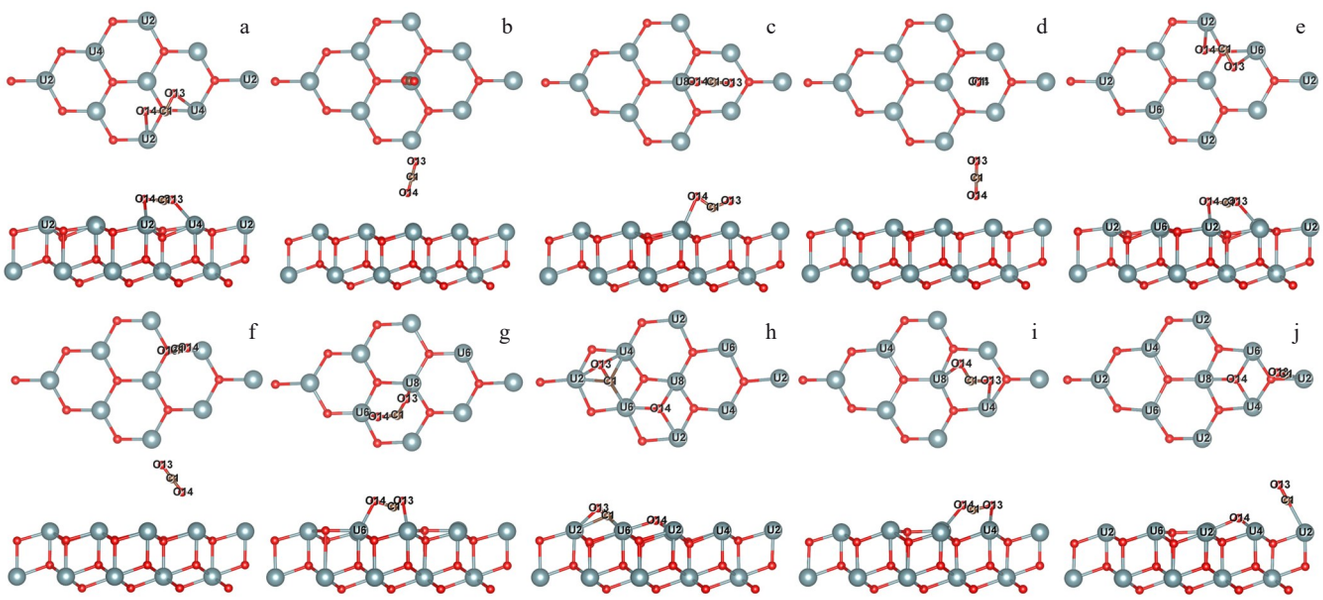

Fig.7 Top and side views of CO_2 molecules with different adsorption configurations on UO_2 (111) slab after structure relaxation: (a) T-Hor; (b) T-Ver; (c) H-Hor; (d) H-Ver; (e) H-down-O-Hor; (f) H-down-O-Ver; (g) B-short-Hor; (h) B-short-Ver; (i) B-long-Hor; (j) B-long-Ver

that CO_2 adsorption is more stable than CO adsorption on the UO_2 (111) slab.

2.4 DOS

Fig. 10 presents TDOS and PDOS of UO_2 (111) slab before and after CO and CO_2 molecule adsorption with the optimal B-short-Ver configuration. Notably, PDOS of the 5f orbital exhibits a sharper profile, compared with that of other orbitals, indicating the strong correlation of uranium 5f electrons. PDOS of U atoms shows hybridization with that of the O atoms whether the adsorption occurs or not. For instance, hybridization exists between the U 6p and O 2s orbitals within the energy range from −25 eV to −15 eV. Similar phenomenon can also be observed between the U 6d/U 5f orbitals and O 2p orbitals within the energy range from − 10 eV to 0 eV. This result illustrates the formation of stable chemical bonds between the U and O atoms in the UO_2 (111) slab. However, a new peak emerges at −10 eV due to the adsorption of CO and CO_2 molecules, as indicated by the black dotted rectangles in Fig.10e and 10f, respectively.

To further investigate the PDOS of specific atoms and orbitals, Fig. 11 displays PDOS of U and O atoms before and after CO and CO_2 molecule adsorption with optimal B-short-

Table 2 Adsorption energy and geometrical parameters of CO_2 molecule adsorption on UO_2 (111) slab

Configuration	E_{ads}/eV	$d_{C\text{-}O1}$/nm	$d_{C\text{-}O2}$/nm	$\theta_{O\text{-}C\text{-}O}$/(°)	Bond C	$d_{Bond\ C}$/nm	Bond O	$d_{Bond\ O}$/nm
T-Hor	−2.368	0.1327	0.1317	115.433	-	-	O_1-U_4	0.2554
					-	-	O_2-U_2	0.2566
T-Ver	0.285	0.1171	0.1182	178.988	-	-	-	-
H-Hor	−1.986	0.1301	0.1290	124.797	-	-	O_2-U_8	0.2463
H-Ver	0.040	0.1166	0.1193	179.695	-	-		
H-down-O-Hor	−2.054	0.1320	0.1318	115.685	-	-	O_1-U_6	0.2545
					-	-	O_2-U_2	0.2555
H-down-O-Ver	0.600	0.1171	0.1184	178.650	-	-	-	-
B-short-Hor	−2.452	0.1331	0.1329	115.460	-	-	O_1-U_8	0.2297
					-	-	O_2-U_6	0.2295
B-short-Ver	−3.824	0.1383	0.3787	-	C-U_2	0.2447	O_1-U_2	0.2395
					C-U_4	0.2464	O_1-U_4	0.2452
					C-U_6	0.2282	O_2-U_2	0.2391
					-	-	O_2-U_6	0.2343
					-	-	O_2-U_8	0.2258
B-long-Hor	−2.862	0.1342	0.1341	115.412	-	-	O_1-U_4	0.2482
					-	-	O_2-U_8	0.2482
B-long-Ver	−3.383	0.1184	0.3506	-	C-U_2	0.2520	O_2-U_4	0.2332
					-	-	O_2-U_6	0.2336
					-	-	O_2-U_8	0.2313

Table 3 Net charge distribution number of CO molecule adsorption on UO_2 (111) slab (e)

Configuration	q_C	q_O	$q_{total\ CO}$	q_{1st}	q_{2nd}	q_{3rd}	q_{4th}	q_{5th}
Atom	−1.0568	1.0568	0	-	-	-	-	-
Free surface	-	-	-	−5.7809	5.5286	5.2625	−10.2094	5.1515
T-Hor	0.6600	1.1792	1.8392	−7.4524	5.4363	5.1804	−10.1723	5.1327
T-Ver	−0.5031	1.0317	0.5286	−6.4080	5.4877	5.2873	−10.0925	5.1531
T-Ver-O	−1.0984	1.2239	0.1255	−5.8113	5.4604	5.2472	−10.2047	5.1356
H-Hor	0.6848	1.1701	1.8549	−7.4156	5.3976	5.1754	−10.1940	5.1345
H-Ver	0.6048	1.1899	1.7947	−7.3581	5.3940	5.1879	−10.1974	5.1367
H-Ver-O	0.5882	1.1856	1.7738	−7.3089	5.4052	5.1866	−10.2364	5.1356
H-down-O-Hor	0.2962	1.2592	1.5554	−7.4138	5.4520	5.2718	−10.0572	5.1461
H-down-O-Ver	−0.2209	1.0279	0.8070	−6.5216	5.4497	5.2343	−10.1576	5.1454
H-down-O-Ver-O	−1.1313	1.1653	0.0340	−5.6998	5.4218	5.2419	−10.1829	5.1351
B-short-Hor	0.6705	1.1672	1.8377	−7.3390	5.3827	5.1680	−10.2278	5.1340
B-short-Ver	0.5944	1.1835	1.7779	−7.4065	5.3999	5.1929	−10.1535	5.1450
B-short-Ver-O	0.3524	1.2325	1.5849	−7.1995	5.4297	5.2231	−10.2161	5.1326
B-long-Hor	0.3012	1.2582	1.5594	−7.4980	5.4542	5.2414	−9.9395	5.1373
B-long-Ver	0.6344	1.1601	1.7945	−7.2402	5.3587	5.1764	−10.2695	5.1362
B-long-Ver-O	0.3460	1.2108	1.5568	−7.1631	5.4145	5.2120	−10.2028	5.1379

Ver configuration. According to Fig. 11, PDOS of U and O atoms represent that of surface atoms of UO_2 (111) slab and CO or CO_2 molecule, respectively. The adsorption of CO and CO_2 molecules results in three hybridization peaks: at −10 eV, within the energy range from −7.5 eV to −2.5 eV, and within the energy range from − 2.5 eV to 0 eV. The first peak primarily involves the hybridization of U 6d, O 2p, and C 2p orbitals, contributing to the newly formed peaks in Fig. 10e and 10f. The peak value of the O 2p orbital is higher than that of the C 2p orbital. The second peak is hybridized by U 6d, O 2p, and C 2p orbitals, and the participation of the O 2p orbital is more obvious than that of the C 2p orbital, as determined by the area enclosed by PDOS of atomic orbitals and coordinate axis. The third peak primarily results from the hybridization of

Table 4 Net charge distribution number of CO_2 molecule adsorption on UO_2 (111) slab (e)

Configuration	q_{O1}	q_{O2}	q_C	$q_{total\ CO_2}$	q_{1st}	q_{2nd}	q_{3rd}	q_{4th}	q_{5th}
Atom	1.0452	1.0452	−2.0904	0	-	-	-	-	-
Free surface	-	-	-	-	−5.7809	5.5286	5.2625	−10.2094	5.1515
T-Hor	1.2217	1.2465	−0.9422	1.5260	−7.4997	5.4123	5.2619	−9.8849	5.1410
T-Ver	1.0061	1.1935	−2.1003	0.0993	−5.7858	5.4470	5.2493	−10.1981	5.1389
H-Hor	1.1986	1.1639	−0.9309	1.4316	−7.2936	5.4152	5.2306	−9.9683	5.1410
H-Ver	0.9567	1.2330	−2.0554	0.1343	−6.0756	5.4895	5.2746	−10.0244	5.1538
H-down-O-Hor	1.2113	1.2083	−0.9111	1.5085	−7.5495	5.4512	5.3020	−9.9160	5.1607
H-down-O-Ver	1.0491	1.1961	−2.1205	0.1247	−5.8550	5.4517	5.2520	−10.1608	5.1401
B-short-Hor	1.1926	1.1950	−0.7854	1.6022	−7.5898	5.3988	5.2619	−9.8580	5.1438
B-short-Ver	1.1460	1.2675	0.6408	3.0543	−8.4446	5.2653	5.1609	−10.2081	5.1306
B-long-Hor	1.1885	1.1861	−0.6193	1.7553	−7.4667	5.3945	5.2263	−10.0992	5.1472
B-long-Ver	1.1045	1.3106	−0.4477	1.9674	−7.7005	5.4568	5.2142	−10.1260	5.1421

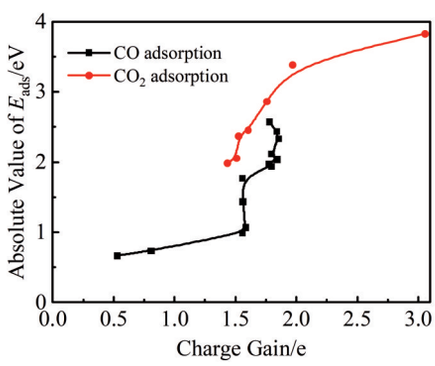

Fig.8 Relationship between absolute value of adsorption energy E_{ads} and charge gain in CO and CO_2 molecule adsorption on UO_2 (111) slab

U 6d, U 5f, O 2p or O1 2p, and C 2p orbitals. The participation order of this peak formation is as follows: U 5f, U 6d, C 2p, and O 2p/O1 2p, which indicates that the peak is predominantly formed by the bonding between C and surface U atoms. Notably, the participation of the O2 2p orbital is significantly less obvious than that of other orbitals in the formation of the hybridized peak at − 10 eV and within the energy range from −2.5 eV to 0 eV, owing to the dissociation between the O2 and C atoms after CO adsorption with B-short-Ver configuration.

2.5 AIMD simulation

The abovementioned adsorption calculations were conducted at the circumstance temperature of 0 K. However, it is impossible to approach 0 K in practical experiments. Therefore, the adsorption evolution was investigated based on CO and CO_2 molecule adsorption with typical configurations on UO_2 (111) slab at the room temperature (300 K). The typical configurations include B-short-Ver configuration for CO adsorption as well as B-short-Ver and B-long-Ver configurations for CO_2 adsorption. B-short-Ver configuration is the optimal configuration for CO molecule adsorption, whereas the B-short-Ver and B-long-Ver configurations are dissociated after CO_2 molecule adsorption. Fig. 12 – Fig. 14 show the structure evolution and charge density difference in the CO adsorption with B-short-Ver configuration and CO_2 adsorption with B-short-Ver and B-long-Ver configurations on UO_2 (111) slab at 300 K by AIMD simulation. Yellow area indicates the increase in charge density (isosurface level: 10 e/nm^3), and blue area indicates the decrease in charge density (isosurface level: 4 e/nm^3). Blue-gray, brown, and red balls represent the uranium, carbon, and oxygen atoms, respectively.

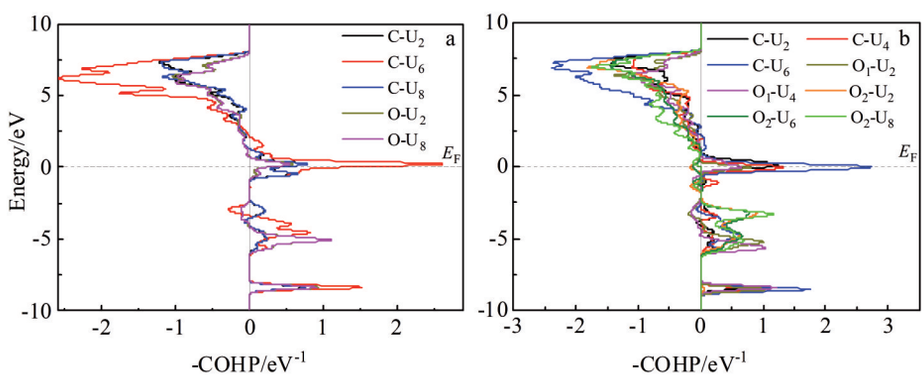

Fig.9 COHP values of C and O atoms with surface atoms in CO (a) and CO_2 (b) molecule adsorption with optimal B-short-Ver configuration

Table 5 ICOHP values for C and O with surface atoms in CO and CO_2 molecule adsorption with optimal B-short-Ver configuration on UO_2 (111) slab

Configuration	Bond C	ICOHP-C/eV	Bond O	ICOHP-O/eV
B-short-Ver/CO	C-U_2	2.8509	O-U_2	2.5309
	C-U_6	5.8475	O-U_8	2.4953
	C-U_8	2.8348	-	-
B-short-Ver/CO_2	C-U_2	3.0719	O_1-U_2	2.9757
	C-U_4	3.1276	O_1-U_4	2.6981
	C-U_6	6.1249	O_2-U_2	3.7216
	-	-	O_2-U_6	4.1059
	-	-	O_2-U_8	4.9308

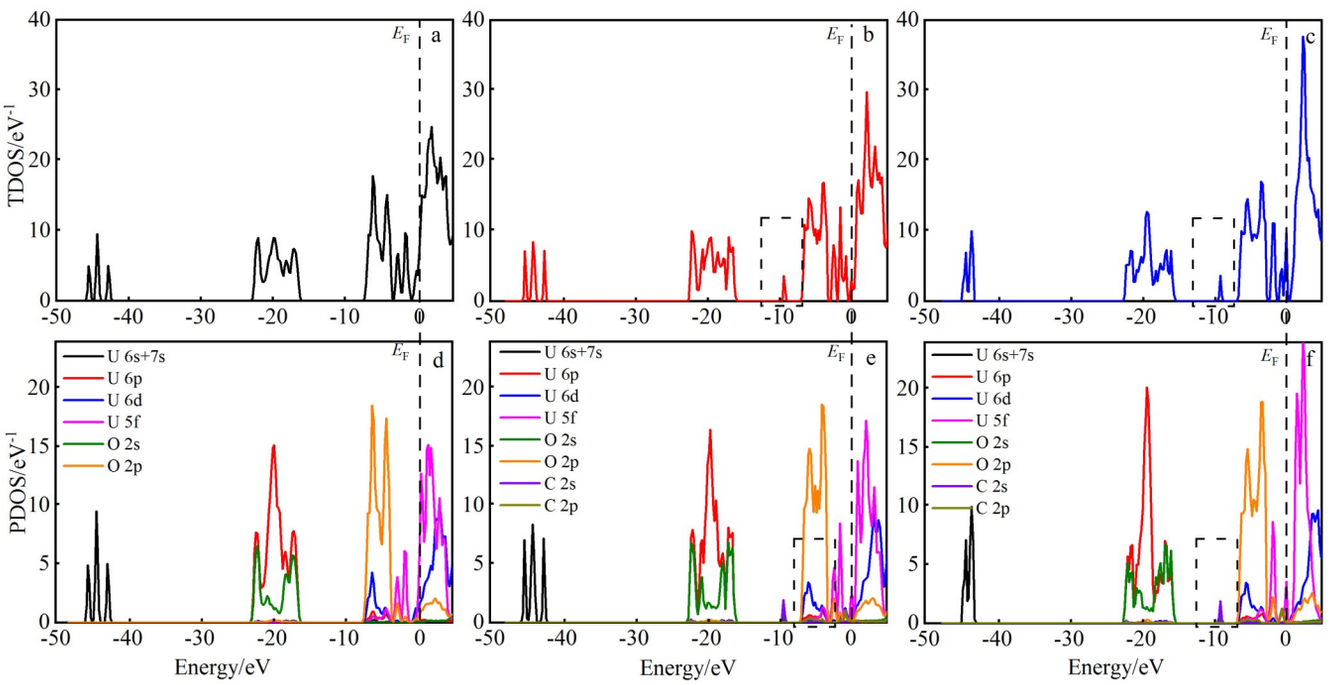

Fig.10 TDOS (a–c) and PDOS (d–f) of UO_2 (111) slab before (a, d) and after CO (b, e) and CO_2 (c, f) molecule adsorption with optimal B-short-Ver configuration

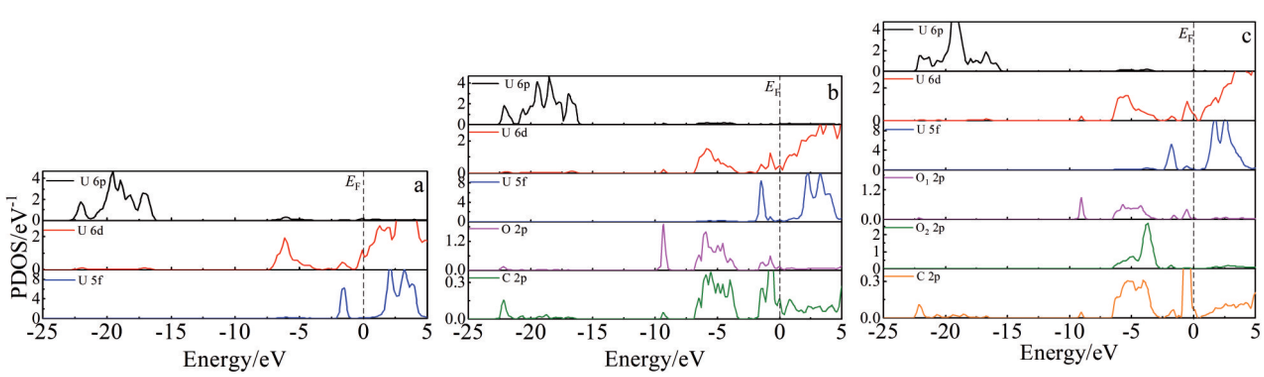

Fig.11 PDOS of specific atoms and orbitals before (a) after CO (b) and CO_2 (c) molecule adsorption with optimal B-short-Ver configuration

Verlet algorithm was performed in AIMD calculations based on NVT ensemble. Then, the total calculation time was 1000 fs with time scale of 1 fs. Besides, Langevin thermostat[48–50] was applied for AIMD simulation, suggesting that the temperature can be maintained by modifying the Newton equations of motion[48], as follows:

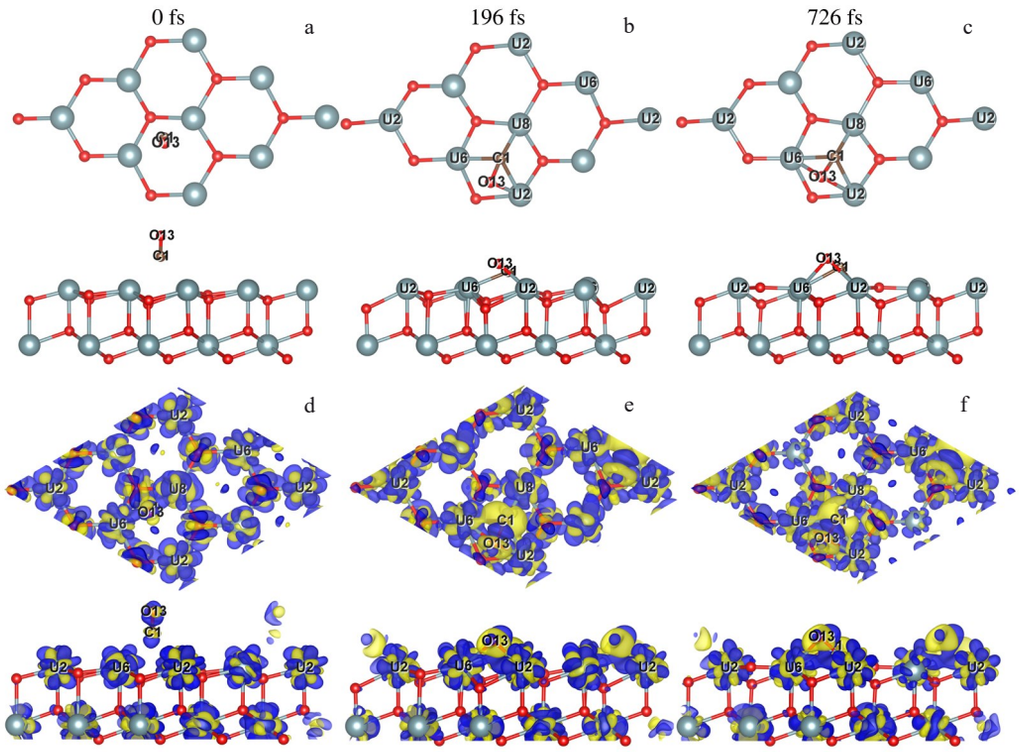

Fig.12 Side and top views of structure evolution (a–c) and charge density difference (d–f) in CO adsorption with B-short-Ver configuration on UO_2 (111) slab at 300 K

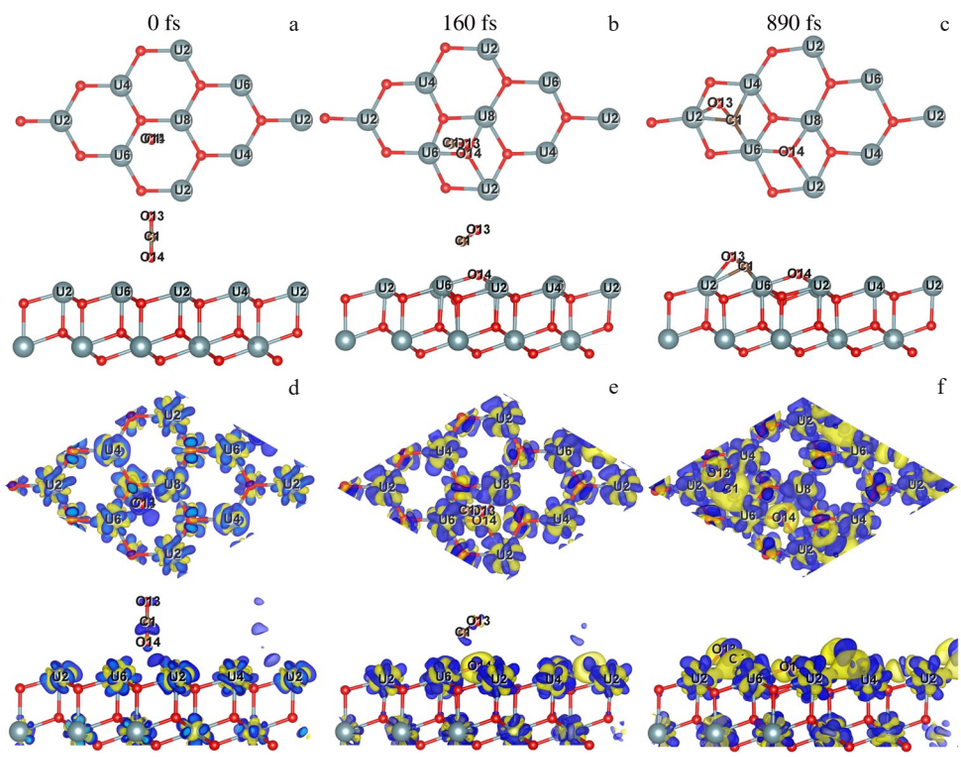

Fig.13 Side and top views of structure evolution (a–c) and charge density difference (d–f) in CO_2 adsorption with B-short-Ver configuration on UO_2 (111) slab at 300 K

$$\dot{r}_i = p_i/m_i \quad (2)$$

$$\dot{p}_i = F_i - \gamma_i p_i + f_i \quad (3)$$

where p_i is the atom momenta; F_i is the force acting on atom i owing to the interaction potential; γ_i is friction coefficient; f_i is

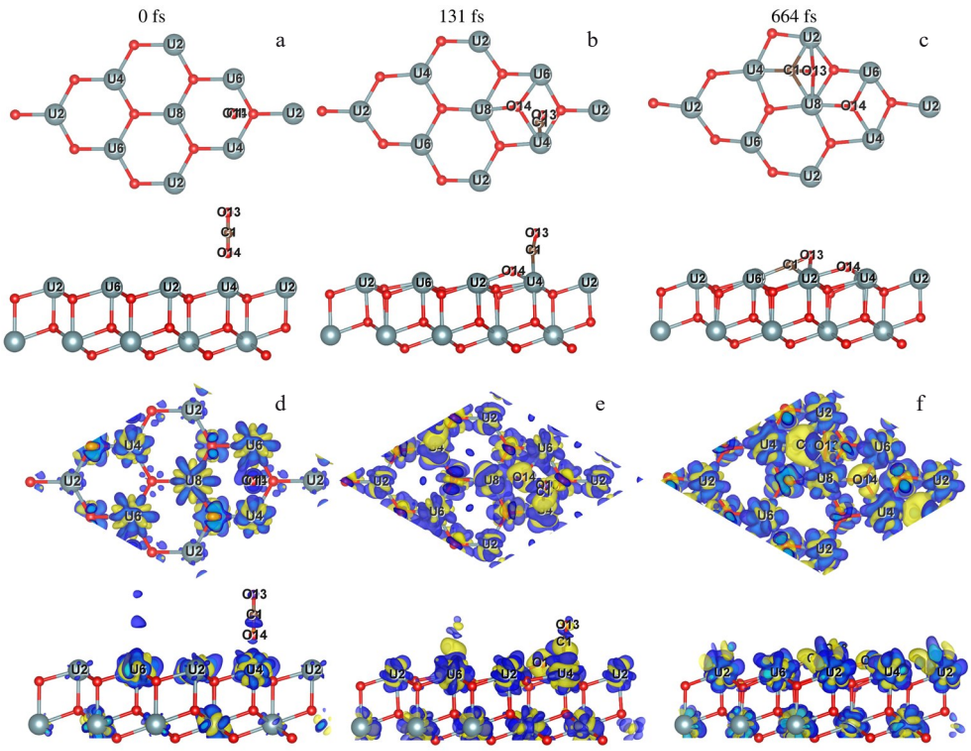

Fig.14 Side and top views of structure evolution (a–c) and charge density difference (d–f) in CO_2 adsorption with B-long-Ver configuration on UO_2 (111) slab at 300 K

the random force with the dispersion σ_i. The dispersion σ_i corresponds to the friction coefficient γ_i[48] and it can be expressed by Eq.(4), as follows:

$$\sigma_i^2 = 2m_i\gamma_i k_B T/\Delta t \quad (4)$$

where k_B is the Boltzmann constant; Δt is the time-step used in molecular dynamics to integrate the equations of motion; T is temperature. Structure differences can be observed in the adsorption configurations between the stable configurations at 300 K and the selected configurations at 0 K. However, at 300 or 0 K, CO_2 molecules undergo dissociation in the B-short-Ver and B-long-Ver configurations. According to Fig. 12–Fig. 14, the C and O atoms are located in the yellow areas, whereas the U atoms of the UO_2 (111) slab are in the blue areas. The size of these surrounding areas is increasesd with prolonging the reaction time, indicating the increase in charge transfer. Ultimately, stable chemical bonds are formed between the CO/CO_2 molecules and the UO_2 (111) slab, as inferred by the evolution of the charge density difference[51] in Fig.12–Fig.14. A conformation similar to the final adsorption result of CO molecule adsorption on the UO_2 (111) slab can be observed at 196 fs. Therefore, for the B-short-Ver and B-long-Ver configurations, CO_2 molecules undergo dissociation at 160 and 131 fs, respectively. The primary reaction of CO and CO_2 adsorption on the UO_2 (111) slab at 300 K occurs within 200 fs in the whole process.

3 Conclusions

1) UO_2 is treated as a non-metallic material with calculated band gap of 1.84 eV, which is slightly smaller than the experiment value of 2.1 eV.

2) The adsorption stability of the bridge site is better than that of the top and hollow sites in the CO and CO_2 molecule adsorption on UO_2 (111) slab. Considering the charge transfer, CO adsorption exhibits better stability than CO_2 adsorption does. The adsorption types include stable (chemical and physical) and unstable adsorption for CO molecules. The stability of CO_2 adsorption with optimal configuration is better than that of CO adsorption.

3) B-short-Ver configuration is the optimal adsorption configuration for both CO and CO_2 molecule adsorption on the UO_2 (111) slab. CO_2 molecules are dissociated in the B-short-Ver and B-long-Ver configurations.

4) The antibonding orbitals of CO and CO_2 molecules are filled by transferred electrons from the surface U atoms through C atoms.

5) U atoms hybridize with the C and O atoms of CO and CO_2 molecules, resulting in three hybridization peaks: the peak at −10 eV, which is caused by the hybridization of U 6d, O 2p, and C 2p orbitals; within the energy range from −7.5 eV to −2.5 eV, which is caused by the hybridization of U 6d, O 2p, and C 2p orbitals; within the energy range from −2.5 eV to 0 eV, which is caused by the hybridization of U 6d, U 5f, O 2p or O1 2p, and C 2p orbitals.

6) CO_2 molecules are dissociated in the B-short-Ver and B-long-Ver configurations, which is consistent with the dissociation at 0 K. The adsorption of CO and CO_2 molecules on the UO_2 (111) slab primarily occurs within 200 fs.

References

1 Fink J K, Chasanov M G, Leibowitz L. *Journal of Nuclear Materials*[J], 1981, 102(1–2): 17

2 Yan C, Yu X H, Huang H *et al*. *Annals of Nuclear Energy*[J], 2022, 171: 109044

3 Zhang Y F, Hansen E D, Harbison T *et al*. *Journal of the American Ceramic Society*[J], 2022, 105(6): 4471

4 Zhou S X, Ma H, Xiao E D *et al*. *Physical Review B*[J], 2022, 106(12): 125134

5 Nadeau J S. *Journal of the American Ceramic Society*[J], 1969, 52(1): 1

6 Manara D, Ronchi C, Sheindlin M *et al*. *Journal of Nuclear Materials*[J], 2005, 342(1–3): 148

7 Wang B T, Zhang P, Lizárraga R *et al*. *Physical Review B*[J], 2013, 88(10): 104107

8 Maugeri E, Wiss T, Hiernaut J P *et al*. *Journal of Nuclear Materials*[J], 2009, 385(2): 461

9 Frigerio G, Gerevini T. *Journal of Nuclear Materials*[J], 1965, 16(1): 76

10 Thompson A E, Wolverton C. *Physical Review B*[J], 2011, 84(13): 134111

11 Adams J B, Wolfer W G, Foiles S M *et al*. *Fundamental Aspects of Inert Gases in Solids*[M]. New York: Plenum Press, 1991: 3

12 Chong S V, Barteau M A, Idriss H. *Surface Science Spectra*[J], 2001, 8(4): 297

13 Petit T, Freyss M, Garcia P *et al*. *Journal of Nuclear Materials*[J], 2003, 320(1–2): 133

14 Geng H Y, Chen Y, Kaneta Y *et al*. *Physical Review B*[J], 2010, 82(9): 094106

15 Sandberg R L, Allred D D, Lunt S *et al*. *Optical Science and Technology: SPIE 49th Annual Meeting*[C]. Denver: SPIE, 2004, 5538: 107

16 Chen Q Y, Lai X C, Tang T *et al*. *Journal of Nuclear Materials*[J], 2010, 401(1–3): 118

17 Söderlind P, Eriksson O, Johansson B *et al*. *Nature*[J], 1995, 374(6522): 524

18 Weck P F, Kim E, Jové-Colón C F *et al*. *Dalton Transactions*[J], 2013, 42(2): 457

19 Li J W, Jia W M, Lv S S *et al*. *Rare Metal Materials and Engineering*[J], 2023, 52(5): 1650

20 Asada K, Ono K, Yamaguchi K *et al*. *Journal of Alloys and Compounds*[J], 1995, 231(1–2): 780

21 Leenaers A, Sannen L, Van den Berghe S *et al*. *Journal of Nuclear Materials*[J], 2003, 317(2–3): 226

22 Sattonnay G, Ardois C, Corbel C *et al*. *Journal of Nuclear Materials*[J], 2001, 288(1): 11

23 Wen X D, Martin R L, Henderson T M *et al*. *Chemical Reviews*[J], 2013, 113(2): 1063

24 Petit L, Svane A, Szotek Z *et al*. *Physical Review B*[J], 2010, 81(4): 045108

25 Sun Y P, Xia X B, Qiao Y B *et al*. *Science China Materials*[J], 2016, 4(59): 279

26 Dorado B, Jomard G, Freyss M *et al*. *Physical Review B*[J], 2010, 82(3): 035114

27 Skomurski F N, Ewing R C, Rohl A L *et al*. *American Mineralogist*[J], 2006, 91(11–12): 1761

28 Huda M N, Ray A K. *International Journal of Quantum Chemistry*[J], 2005, 102(1): 98

29 Skomurski F N, Shuller L C, Ewing R C *et al*. *Journal of Nuclear Materials*[J], 2008, 375(3): 290

30 Rák Z, Ewing R C, Becker U. *Surface Science*[J], 2013, 608: 180

31 Kresse G, Hafner J. *Physical Review B*[J], 1993, 48(17): 13115

32 Kresse G, Furthmüller J. *Computational Materials Science*[J], 1996, 6(1): 15

33 Perdew J P, Burke K, Ernzerhof M. *Physical Review Letters*[J], 1996, 77(18): 3865

34 Kresse G, Joubert D. *Physical Review B*[J], 1999, 59(3): 1758

35 Watanabe T, Srivilliputhur S G, Schelling P K *et al*. *Journal of the American Ceramic Society*[J], 2009, 92(4): 850

36 Monkhorst H J, Pack J D. *Physical Review B*[J], 1976, 13(12): 5188

37 Barrett S A, Jacobson A J, Tofield B C *et al*. *Acta Crystallographica Section B: Structural Crystallography and Crystal Chemistry*[J], 1982, 38(11): 2775

38 Gupta F, Brillant G, Pasturel A. *Philosophical Magazine*[J], 2007, 87(17): 2561

39 Scheu C, Dehm G, Kaplan W D *et al*. *Physica Status Solidi A*[J], 1998, 166(1): 241

40 Nerikar P, Watanabe T, Tulenko J S *et al*. *Journal of Nuclear Materials*[J], 2009, 384(1): 61

41 Schoenes J. *Journal of Applied Physics*[J], 1978, 49(3): 1463

42 Schwarz G, Kley A, Neugebauer J *et al*. *Physical Review B*[J], 1998, 58(3): 1392

43 Ogren P J. *Journal of Chemical Education*[J], 2002, 79(1): 117

44 Austin A E. *Acta Crystallographica*[J], 1959, 12(2): 159

45 Deringer V L, Tchougréeff A L, Dronskowski R. *The Journal of Physical Chemistry A*[J], 2011, 115(21): 5461

46 Maintz S, Deringer V L, Tchougréeff A L *et al*. *Journal of Computational Chemistry*[J], 2016, 37(11): 1030

47 Nelson R, Ertural C, George J *et al*. *Journal of Computational Chemistry*[J], 2020, 41(21): 1931

48 Allen M P, Tildesley D J. *Computer Simulation of Liquids*[M]. New York: Oxford University Press, 1991

49 Hoover W G, Ladd A J C, Moran B. *Physical Review B*[J], 1982, 48(26): 1818

50 Evans D J. *The Journal of Chemical Physics*[J], 1983, 78(6): 3297

51 Momma K, Izumi F. *Journal of Applied Crystallography*[J], 2008, 41(3): 653

CO和CO_2在UO_2 (111)表面吸附和解离的第一性原理和分子动力学研究

李俊炜[1,2]，贾维敏[2]，刘　崇[1]，李沛尧[1]，李正操[1]

(1. 清华大学 材料学院，北京 100084)

(2. 西安高科技研究所，陕西 西安 710025)

摘　要：基于密度泛函理论（DFT）的第一性原理计算，在计算中加入Hubbard项进行校正，探究了CO和CO_2分子在UO_2 (111)表面的吸附和解离，分析了不同构型下的静态和动态吸附机理，吸附位点包括顶位、空位、桥位。在静态计算中，探究了吸附过程中多种吸附参数的变化，如吸附构型、吸附能、电荷转移等。利用第一性原理分子动力学（AIMD），探究了特定构型下CO_2分子的解离过程及差分电荷密度变化。结果表明，CO分子的吸附可分为2种类型：（1）自发吸附，包括化学和物理吸附；（2）非自发吸附。CO_2分子的吸附仅表现为自发吸附的化学吸附及非自发吸附，无物理吸附。CO和CO_2分子的最优吸附构型均为短桥位垂直（B-short-Ver）吸附。此外，0 K下CO_2分子在UO_2 (111)表面的B-short-Ver和长桥位垂直吸附构型吸附后会自发解离。AIMD模拟结果表明，这2种构型在300 K下均发生解离。

关键词：二氧化铀；化学吸附；DFT+U；桥位垂直

作者简介：李俊炜，男，1997年生，博士生，清华大学材料学院，北京 100084，E-mail：lijunwei21@mails.tsinghua.edu.cn